

# DNA handles bias force-dependent looping times

Wout Laeremans,<sup>1</sup> Jef Hooyberghs,<sup>2</sup> and Wouter G. Ellenbroek<sup>1,\*</sup>

<sup>1</sup>*Soft Matter and Biological Physics, Department of Applied Physics and Science Education, and Institute for Complex Molecular Systems, Eindhoven University of Technology, P.O. Box 513, 5600 MB Eindhoven, Netherlands*

<sup>2</sup>*UHasselt, Faculty of Sciences, Data Science Institute, Theory Lab, Agoralaan, 3590 Diepenbeek, Belgium*

(Dated: July 9, 2026)

DNA loop formation is a key mechanism in gene regulation, and looping kinetics are sensitive to mechanical tension acting on the DNA. In both single-molecule experiments and biological settings, this tension is typically transmitted through DNA segments flanking the looping region, rather than acting directly at the looping sites. How this indirect force transmission affects the looping time has not been systematically investigated. Using molecular dynamics simulations of a wormlike chain, we show that such flanking segments significantly steepen the force dependence of the looping time, an effect that is insensitive to their length once it exceeds the persistence length, and vanishes when the junction to the looping region is made flexible. We develop an analytical framework that accounts for this effect through a force-dependent shift in the effective free energy landscape of the looping segment. In the limit of small forces, this shift reduces to a zero-force equilibrium average, after which the entire force dependence of the looping time follows analytically. Applying this framework using a coarse-grained DNA model that treats individual bases as rigid bodies, we obtain predictions in quantitative agreement with experimental looping data. Our results demonstrate that the geometry of force transmission has a significant and predictable effect on looping kinetics, with direct implications for the interpretation of tension-dependent looping in both single-molecule experiments and gene regulatory contexts.

## I. INTRODUCTION

Single-molecule force spectroscopy has become an indispensable tool for probing the mechanics and dynamics of biomolecules at the nanoscale [1, 2]. Optical and magnetic tweezers, in particular, have enabled direct measurements of force-extension relations [3], torsional stiffness [4], and looping and unfolding kinetics [5–7] for nucleic acids and proteins. A unifying theoretical framework for interpreting these experiments is the effective free energy landscape: by projecting the high-dimensional conformational dynamics of a polymer onto a single reaction coordinate, typically the end-to-end distance  $r$ , one obtains a one-dimensional diffusion problem whose barrier height directly determines the timescale of the process of interest [8–11].

A particularly important application is DNA looping, which plays a central role in gene regulation [12]. Loop formation brings two specific binding sites into contact, and its kinetics are sensitive to the mechanical tension acting on the DNA [5, 12–14]. Such tension arises both in single-molecule experiments and in biological contexts, where DNA is subject to forces from, for example, molecular motors, supercoiling, or chromatin organisation [12, 14–18]. The relevance of this question is reinforced by a growing body of work proposing that chromatin loops themselves may form through the passive diffusive capture of anchor sites, rather than through active, motor-driven extrusion [19, 20], which would place the diffusion-limited looping kinetics considered here directly at the heart of chromosome organisation. Crucially, in all settings the tension acts globally on the DNA rather than specifically at the looping sites: the flanking DNA segments transmit the force to the looping region indirectly. In optical-tweezer

experiments this is made explicit by the use of DNA handles that connect the binding sites to the trapped beads, as illustrated in Fig. 1. The standard theoretical framework for looping kinetics under force assumes that the tension acts directly at the ends of the looping segment [10, 11, 13, 21], which is never strictly the case in practice. How this indirect force transmission affects the looping time has not been systematically investigated.

Here we ask, and answer, a precise question: how do flanking DNA segments bias the force dependence of the looping time, and how can this effect be captured theoretically? Using molecular dynamics simulations, we first demonstrate that handles of a length close to the persistence length cause the looping time to increase substantially more steeply with force than the standard theory predicts, that this effect saturates once the handle length exceeds the persistence length, and that it disappears entirely when the junction is made flexible. We trace all of these observations back to modifications of the effective free energy landscape of the looping segment, and develop a theoretical framework that quantitatively predicts the handle-induced changes in DNA looping times.

This is particularly relevant in the experimentally relevant regime where the handles are long compared to the persistence length. In this case, their effect simplifies considerably and can be absorbed into an effective description of the looping segment. This yields a modified free energy landscape that captures indirect force transmission and can be used directly to predict DNA looping times within standard kinetic frameworks. In the small-force limit, the theory depends only on a zero-force equilibrium property, which determines the full force dependence of the looping time and enables direct quantitative comparison with experimental measurements.

The paper is organised as follows. Section II reviews the free energy landscape of a wormlike chain without handles. Section III introduces the looping time formula, presents the simulation results, and establishes the failure of the standard

\* w.g.ellenbroek@tue.nl

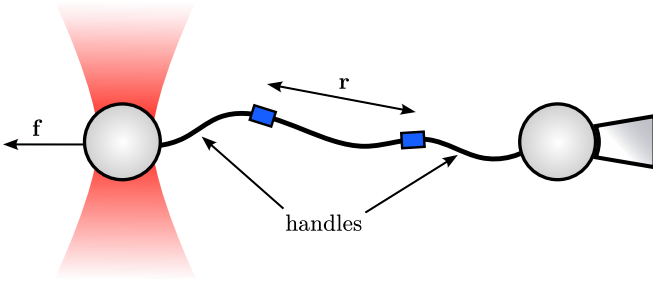


Figure 1. Schematic of a DNA looping experiment in an optical-tweezer setup. One bead is held in an optical trap (red), while the other bead is immobilized by a micropipette. An external force  $\mathbf{f}$  is applied by displacing the optical trap relative to the fixed bead, thereby stretching the DNA tether. The DNA construct consists of an interior segment with end-to-end distance  $r$ , defined as the region between two specific binding sites (blue squares). This segment is flanked by inert DNA handles that connect the binding sites to the beads. The looping reaction occurs exclusively within the interior segment, while the handles act as mechanical transducers of the applied force.

theory in the presence of handles. The theoretical framework including handles is developed in Sec. IV, and the small-force expansion in Sec. V. Section VI applies the theory to the cgDNA+ model and compares to experimental data. We conclude in Sec. VII.

## II. EQUILIBRIUM STATISTICS OF A WORMLIKE CHAIN WITHOUT HANDLES

We begin by reviewing the theoretical framework for the free energy landscape of a semiflexible polymer in the absence of handles, as this provides the baseline against which the effect of handles is assessed. We model the polymer as a wormlike chain (WLC) [22, 23], the standard continuum description of semiflexible biopolymers such as double-stranded DNA. The polymer has contour length  $L$  and is characterised by a unit tangent field  $\mathbf{t}(s)$ , with curvilinear distance  $s \in [0, L]$ . In the absence of an applied force, the Hamiltonian reads

$$\beta \mathcal{H}_0[\mathbf{t}] = \frac{\ell_p}{2} \int_0^L |\partial_s \mathbf{t}(s)|^2 ds, \quad (1)$$

where  $\beta^{-1} = k_B T$  is the thermal energy and  $\ell_p$  the persistence length. The end-to-end vector is

$$\mathbf{r}[\mathbf{t}] = \int_0^L \mathbf{t}(s) ds. \quad (2)$$

When a constant force  $\mathbf{f}$  is applied, as in an optical-tweezer experiment, the Hamiltonian acquires an additional mechanical work term,

$$\beta \mathcal{H}_f[\mathbf{t}] = \beta \mathcal{H}_0[\mathbf{t}] - \beta \mathbf{f} \cdot \mathbf{r}[\mathbf{t}]. \quad (3)$$

## Probability density of the end-to-end distance

The probability density of observing a given end-to-end vector  $\mathbf{r}$  at force  $\mathbf{f}$  is obtained from the path integral

$$P(\mathbf{r}; \mathbf{f}) = \frac{\int \mathcal{D}[\mathbf{t}] \delta(\mathbf{r} - \mathbf{r}[\mathbf{t}]) e^{-\beta \mathcal{H}_f[\mathbf{t}]} d\mathbf{t}}{\int \mathcal{D}[\mathbf{t}] e^{-\beta \mathcal{H}_f[\mathbf{t}]} d\mathbf{t}}. \quad (4)$$

Denoting the zero-force distribution as  $P_0(\mathbf{r}) \equiv P(\mathbf{r}; \mathbf{f} = 0)$ , the distribution under force can be written in closed form as [11]

$$P(\mathbf{r}; \mathbf{f}) = \frac{P_0(\mathbf{r}) e^{\beta \mathbf{f} \cdot \mathbf{r}}}{\int d^3 r' P_0(\mathbf{r}') e^{\beta \mathbf{f} \cdot \mathbf{r}'}}. \quad (5)$$

Without loss of generality we orient the force along the  $z$ -axis,  $\mathbf{f} = f \hat{\mathbf{z}}$ . At zero force the chain is isotropic, so  $P_0(\mathbf{r}) \sim P_0(r)$  depends only on the end-to-end distance  $r = |\mathbf{r}|$ . Integrating Eq. (5) over the solid angle using  $\mathbf{f} \cdot \mathbf{r} = fr \cos \theta$  gives

$$P(r; f) \propto P_0(r) \int_0^\pi \sin \theta e^{\beta fr \cos \theta} d\theta = P_0(r) \frac{\sinh(\beta fr)}{\beta fr}, \quad (6)$$

so that, after normalisation [11]

$$P(r; f) = \frac{P_0(r) \frac{\sinh(\beta fr)}{\beta fr}}{\int_0^L dr' P_0(r') \frac{\sinh(\beta fr')}{\beta fr'}}. \quad (7)$$

The corresponding effective free energy  $\beta F(r; f) = -\ln P(r; f)$  then satisfies [11]

$$\beta F(r; f) = \beta F(r; 0) - \ln \left[ \frac{\sinh(\beta fr)}{\beta fr} \right]. \quad (8)$$

## Analytic approximation for $P_0(r)$

Equation (8) reduces the finite-force problem to knowledge of the zero-force radial distribution  $P_0(r)$ . No exact closed-form expression exists for the WLC, but several analytical approximations have been proposed [24, 25]. Here we employ the mean-field (MF) approximation of Bhattacharjee *et al.* [25],

$$P_0^{\text{MF}}(r) \propto r^2 \left[ 1 - \left( \frac{r}{L} \right)^2 \right]^{-9/2} \exp \left[ -\frac{3L}{4\ell_p \left( 1 - \left( \frac{r}{L} \right)^2 \right)} \right], \quad (9)$$

which enforces the correct extensibility limit  $r \rightarrow L$  and recovers Gaussian behaviour for  $r \ll L$ . Inserting Eq. (9) into Eq. (8) yields a fully analytic prediction for the free energy at arbitrary force.

Figure 2 illustrates these results for parameters representative of real experiments [5]. The zero-force free energy is extracted from simulation (details in Appendix A) by sampling

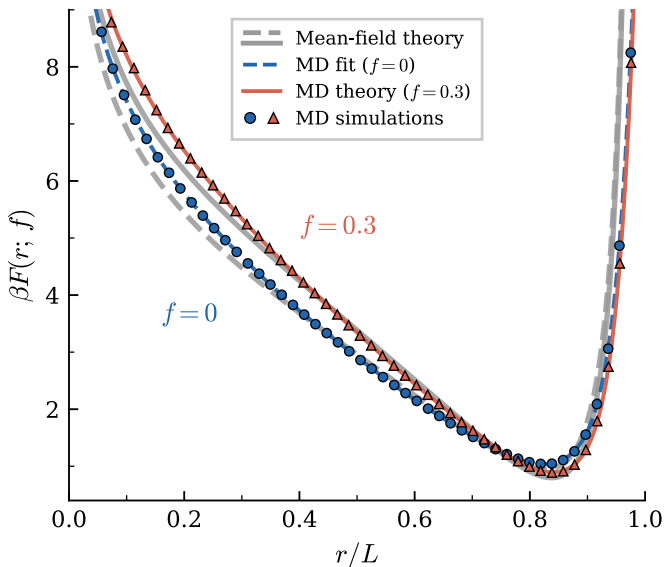


Figure 2. Effect of an applied force on the effective free energy of a wormlike chain (WLC) with contour length  $L = 10.5$  and persistence length  $\ell_p = 5$  (dimensionless units). Blue circles: simulation data at zero force, dashed blue line: 12th-order polynomial fit used as input for Eq. (8). Orange triangles: simulation data at  $f = 0.3$ , full orange line: theoretical prediction from Eq. (8). Grey lines: fully analytical predictions based on the MF distribution, Eq. (9). In physical units (see Ref. [10] for conversion) the system corresponds to a polymer with  $L \approx 105$  nm and  $\ell_p \approx 50$  nm at an applied force  $f \approx 0.12$  pN, representative of DNA looping experiments [5].

end-to-end distances, binning them into a histogram to obtain a probability distribution  $P(r)$ , and computing  $\beta F(r; 0) = -\ln(P(r))$  (blue circles). This is well captured by the polynomial fit (dashed blue line), which is then substituted into Eq. (8) to predict the free energy at  $f = 0.3$  (full orange line). The agreement with the direct simulation at that force (orange triangles) is excellent, confirming the accuracy of the analytic force correction. The MF approximation (grey lines) agrees well with the simulation near the free energy minimum, with deviations becoming visible in the tails. These results establish the theoretical baseline against which the effect of handles is assessed in the following sections.

### III. LOOPING TIMES

The effective free energy  $F(r; f)$  derived in the previous section is not merely a convenient summary of the equilibrium statistics, it also governs the kinetics of polymer looping. The capture radius  $r_c$  represents the maximum end-to-end distance at which the two reactive sites, typically protein binding domains or specific DNA sequences, can form a contact, and is set by the range of the binding interaction. We define the looping time  $\tau(f)$  as the mean first-passage time for the end-to-end distance  $r(t)$  to reach this capture radius  $r_c$  for the first time, starting from a chain that is initially in equilibrium.

Under the assumption that the dynamics of  $r(t)$  can be modelled as overdamped diffusion on the one-dimensional free

energy landscape  $F(r; f)$ , the Szabo–Schulten–Schulten theory [9] gives the mean first-passage time in closed form. The expression to predict the looping time then yields [9, 10]

$$\tau(f) \sim \frac{1}{Z} \int_{r_c}^L dr \int_{r_c}^r dr' \int_{r'}^L dr'' e^{-\beta[F(r; f) - F(r'; f) + F(r''; f)]}, \quad (10)$$

with the partition function

$$Z = \int_{r_c}^L e^{-\beta F(r; f)} dr. \quad (11)$$

The triple integral in Eq. (10) has a transparent physical interpretation: the innermost integral over  $r''$  accumulates the statistical weight of configurations that are yet to reach  $r_c$ , the middle integral over  $r'$  accounts for the ease of thermal excitation away from each such configuration, and the outer integral over  $r$  averages over all starting positions weighted by the Boltzmann factor. As shown in Ref. [11], Eq. (10) is accurate for short, stiff chains satisfying  $L/\ell_p \lesssim 3$ , precisely the regime relevant to DNA looping experiments [5], where the loopable segment is shorter than a few persistence lengths. Finally, because Eq. (10) requires only  $F(r; f)$  as input, the force dependence of  $\tau$  follows directly from Eq. (8) without any additional free parameters, provided the force is applied directly at the chain ends. We now examine what happens when this condition is not met.

#### Effect of handles on the looping time

In a typical optical-tweezer looping setup, the force is not applied directly to the reactive ends of the molecule. Instead, as illustrated in Fig. 1, the polymer of interest is flanked by handles that connect the specific binding sites to the beads held in the optical traps. The loop is formed exclusively between the two binding sites, i.e. within the interior segment of end-to-end distance  $r$ , while the handles remain outside the loop and serve only as mechanical transducers of the applied force. A natural question therefore arises: do these linker segments affect the force dependence of the looping time  $\tau(f)$ ? This is not a priori obvious. On one hand, the handles do not participate in the looping reaction and one might expect them to be irrelevant beyond setting the mechanical boundary conditions. On the other hand, the handles are themselves semiflexible polymers that fluctuate under the applied force, and their conformational statistics are coupled to those of the interior segment through the binding sites, where the tangents must match. To our knowledge, this question has not been systematically addressed.

Figure 3 provides a direct answer. For a chain without handles ( $h = 0$ , blue circles), both the polynomial-fit and mean-field theories agree well with the MD simulations, confirming the validity of Eq. (10) in this regime. When WLC handles of length  $h = \ell_p$  or  $h = 2\ell_p$  are appended to each binding site (orange symbols), however,  $\tau(f)/\tau(0)$  increases substantially more steeply with force, and the no-handle theory severely underestimates the data. The handles therefore have

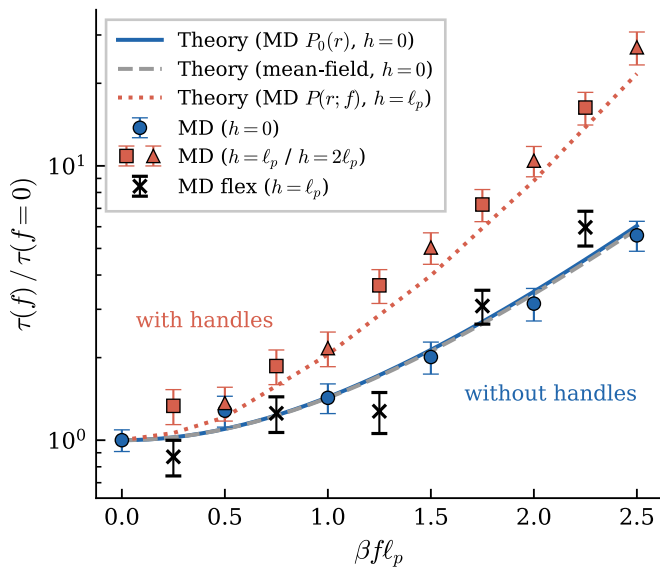


Figure 3. Force dependence of the looping time, normalised by its zero-force value  $\tau(f)/\tau(f=0)$ , as a function of the dimensionless force  $\beta f \ell_p$ . Blue circles: MD simulations without handles ( $h=0$ ). Orange squares and triangles: MD simulations with handles of length  $h=\ell_p$  and  $h=2\ell_p$ , respectively. Blue solid line: theoretical prediction from Eq. (10) using the polynomial fit to  $P_0(r)$ , grey dashed line: same using the MF approximation, Eq. (9). Both theory curves are for  $h=0$ . Orange dotted line: Eq. (10) evaluated using the effective free energy  $F(r; f)$  extracted from MD simulations with handles ( $h=\ell_p$ ). Black crosses: simulations with a flexible (zero bending rigidity) junction between handles and binding sites.

a clear and non-trivial effect on the looping kinetics. Notably, the two handle lengths produce nearly identical results, suggesting that the effect saturates once  $h \gtrsim \ell_p$ . This saturation reflects the exponential decay of tangent-tangent correlations along the handle: when  $h \gg \ell_p$ , the handle orientation decorrelates from  $\mathbf{r}$  beyond an arc-length of order  $\ell_p$  from the attachment point. We will make this picture more precise in Sec. IV.

To test whether this effect can be captured theoretically, we extracted the effective free energy  $F(r; f)$  directly from MD simulations with handles present, using the interior end-to-end distance  $r$  as the reaction coordinate. Inserting this into Eq. (10) yields the orange dotted line, which agrees well with the handle simulations. This confirms that the modified looping time is still fully encoded in the effective free energy. A theoretical prediction of the looping time in the presence of handles therefore reduces to obtaining  $F(r; f)$  for the interior segment when handles are present, which we pursue in the remainder of this work.

Finally, we note that when the junction between the handles and the binding sites is made flexible, meaning when the bending energy penalty at the attachment point is removed, the looping time recovers the no-handle behaviour (black crosses). This is physically natural: without orientational stiffness at the junction, the handles cannot transmit their alignment to the interior segment, effectively decoupling the two. The data show somewhat more scatter around the no-

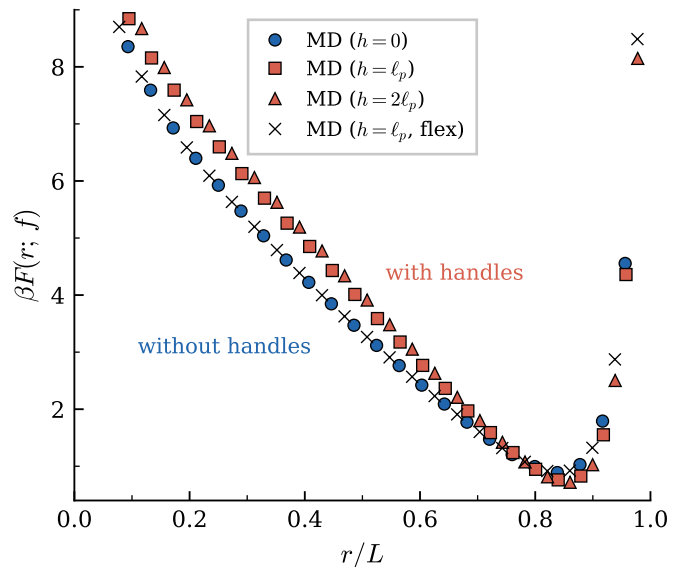


Figure 4. Effective free energy  $\beta F(r; f)$  as a function of the interior end-to-end distance  $r$ , at force  $f=0.3$ . Blue circles: no handles ( $h=0$ ). Orange squares and triangles: WLC handles of length  $h=\ell_p$  and  $h=2\ell_p$ , respectively. Black crosses: flexible-junction handles ( $h=\ell_p$ , zero bending rigidity at the attachment point). The flexible-junction and no-handle curves coincide, as do the two handle curves regardless of length, demonstrating that the handle effect saturates for  $h \gtrsim \ell_p$ .

handle curve, which may reflect the modified conformational dynamics at the flexible junction. Nevertheless, from an experimental perspective, this suggests that replacing the commonly used double-stranded DNA handles with a more flexible polymer, such as single-stranded DNA, could suppress the handle-induced bias in force-dependent looping measurements.

#### IV. EFFECT OF HANDLES ON THE FREE ENERGY LANDSCAPE

The simulation results of Fig. 3 reveal two key observations: the presence of handles significantly steepens the force dependence of the looping time, yet the effect is nearly independent of handle length. These observations find a natural explanation in the effective free energies shown in Fig. 4. The no-handle free energy (blue circles) and the flexible-junction case (black crosses) fall on the same curve, consistent with the looping times being similar in those two cases. The free energies with handles of length  $h=\ell_p$  and  $h=2\ell_p$  (orange squares and triangles) likewise collapse onto a single curve, explaining why the looping time is insensitive to handle length once  $h \gtrsim \ell_p$ .

In Sec. II, the force-dependent free energy was derived for a polymer whose ends coincide with the binding sites. In a setup with handles, as illustrated in Fig. 1, the looping reaction involves only the interior segment of contour length  $L$ , while the applied force acts on the full construct of total length  $L_{\text{tot}} =$

$2h + L$ , where both handles are assumed to have equal length  $h$ . The central question is how the conformational statistics of the interior segment are modified by the flanking handles.

We label the arc length coordinate of the full polymer by  $s \in [0, L_{\text{tot}}]$ , and denote the interior segment by  $s \in [s_0, s_0 + L]$ . Its end-to-end vector is

$$\mathbf{r}[\mathbf{t}] = \int_{s_0}^{s_0+L} \mathbf{t}(s) ds, \quad (12)$$

while the total end-to-end vector decomposes as

$$\mathbf{R}_{\text{tot}}[\mathbf{t}] = \mathbf{r}[\mathbf{t}] + \mathbf{R}_{\text{handles}}[\mathbf{t}], \quad (13)$$

where  $\mathbf{R}_{\text{handles}}[\mathbf{t}] = \int_0^{s_0} \mathbf{t} ds + \int_{s_0+L}^{L_{\text{tot}}} \mathbf{t} ds$  collects the contributions from both handles. Since the force is applied to the ends of the full construct, the Boltzmann weight contains  $e^{\beta \mathbf{f} \cdot \mathbf{R}_{\text{tot}}}$ , and the probability density for the interior segment's end-to-end vector is

$$P(\mathbf{r}; \mathbf{f}) = \frac{\int \mathcal{D}[\mathbf{t}] \delta(\mathbf{r} - \mathbf{r}[\mathbf{t}]) e^{-\beta \mathcal{H}_0[\mathbf{t}] + \beta \mathbf{f} \cdot \mathbf{R}_{\text{tot}}[\mathbf{t}]}}{\int \mathcal{D}[\mathbf{t}] e^{-\beta \mathcal{H}_0[\mathbf{t}] + \beta \mathbf{f} \cdot \mathbf{R}_{\text{tot}}[\mathbf{t}]}}}, \quad (14)$$

where  $\mathcal{H}_0$  is the zero-force WLC Hamiltonian of the full construct. Separating the interior and handle contributions (see Appendix B for the full derivation), Eq. (14) can be rewritten as

$$P(\mathbf{r}; \mathbf{f}) = \frac{P_0(\mathbf{r}) e^{\beta \mathbf{f} \cdot \mathbf{r}} C[\mathbf{r}; \mathbf{f}]}{\int d^3 r' P_0(\mathbf{r}') e^{\beta \mathbf{f} \cdot \mathbf{r}'} C[\mathbf{r}'; \mathbf{f}]}, \quad (15)$$

where the handle correction factor

$$C[\mathbf{r}; \mathbf{f}] = \left\langle e^{\beta \mathbf{f} \cdot \mathbf{R}_{\text{handles}}} \right\rangle_{f=0; \mathbf{r}} \quad (16)$$

is the zero-force conditional average of the handle Boltzmann weight, taken over all chain conformations with the interior segment's end-to-end vector fixed at  $\mathbf{r}$ . Equation (15) has the same structure as the no-handle result, Eq. (5), but is modulated by  $C[\mathbf{r}; \mathbf{f}]$ , which encodes the orientational correlations between the handles and the interior segment. When  $h = 0$ , one has  $C = 1$  identically and the no-handle result is recovered. The key challenge is then to evaluate  $C[\mathbf{r}; \mathbf{f}]$  in a tractable approximation, which we do so below.

### Handle approximation

When  $h \lesssim \ell_p$ , each handle behaves effectively as a rigid rod: thermal fluctuations are insufficient to significantly bend it, so its orientation is strongly correlated with the tangent at the attachment point. On average, and especially at low forces, the handle vector is approximately collinear with  $\mathbf{r}$ , allowing the total end-to-end vector to then be approximated as

$$\mathbf{R}_{\text{tot}} \approx \mathbf{r} + \Delta(r; f) \hat{\mathbf{r}}, \quad (17)$$

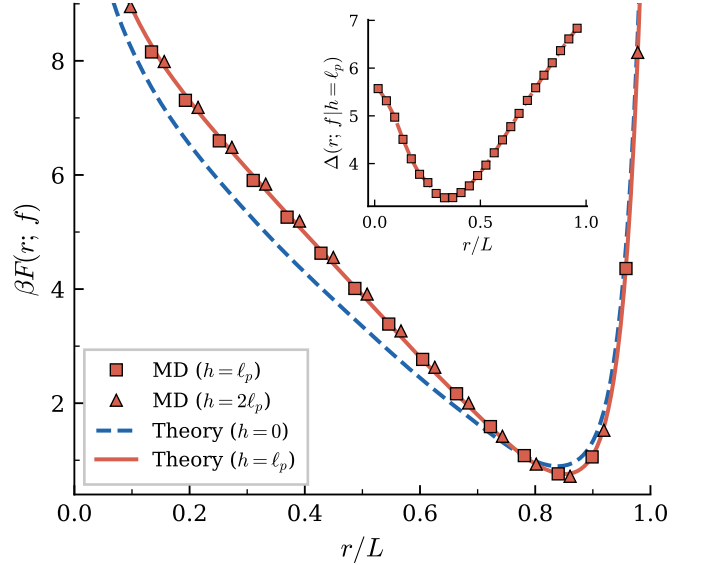


Figure 5. Effective free energy  $\beta F(r; f)$  of the interior segment at force  $f = 0.3$ , with handles of length  $h = \ell_p$  (orange squares) and  $h = 2\ell_p$  (orange triangles). Blue dashed line: theoretical prediction for  $h = 0$  from Eq. (8). Orange solid line: theoretical prediction for  $h = \ell_p$  from Eq. (21) using  $\Delta(r; f | h = \ell_p)$  extracted from MD simulation as input. Inset:  $\Delta(r; f | h = \ell_p)$  as a function of  $r/L$ .

where  $\hat{\mathbf{r}} = \mathbf{r}/r$  and  $\Delta(r; f) \equiv R_{\text{tot}} - r$  is the additional extension contributed by both handles along  $\hat{\mathbf{r}}$ . This alignment assumption is validated in Appendix C, where energy minimization of the chain configurations demonstrates that the inner segment and total direction are indeed strongly aligned across most values of  $r/L$ , particularly at low forces. Since the alignment is valid for most values of  $r/L$ , the approximation in Eq. (17) captures the essential physics of the system. Even more, in Appendix D, it is shown that this assumption is true up to first order in  $f$ . This approximation implies that  $\mathbf{R}_{\text{tot}}$  and  $\mathbf{r}$  subtend the same angle with the force axis, i.e.  $\theta_{\text{tot}} \approx \theta_r$ . The integration over the solid angle then proceeds exactly as in Eq. (6), but with  $r$  replaced by  $r + \Delta(r; f)$ :

$$\begin{aligned} \int d\Omega e^{\beta \mathbf{f} \cdot \mathbf{R}_{\text{tot}}} &= \int_0^\pi d\theta_{\text{tot}} \int_0^{2\pi} d\phi \sin \theta_{\text{tot}} e^{\beta f (r + \Delta(r; f)) \cos \theta_{\text{tot}}} \\ &\approx \int_0^\pi d\theta_r \int_0^{2\pi} d\phi \sin \theta_r e^{\beta f (r + \Delta(r; f)) \cos \theta_r} \\ &= 4\pi \frac{\sinh(\beta f (r + \Delta(r; f)))}{\beta f (r + \Delta(r; f))}. \end{aligned} \quad (18)$$

The radial distribution of the interior segment therefore takes the form

$$P(r; f | h \lesssim \ell_p) = \frac{P_0(r) \frac{\sinh(\beta f (r + \Delta(r; f)))}{\beta f (r + \Delta(r; f))}}{Z(f)}, \quad (19)$$

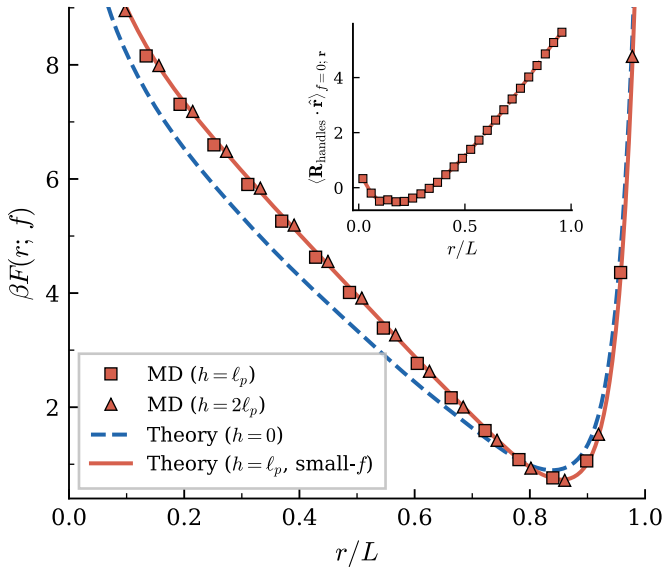


Figure 6. Effective free energy  $\beta F(r; f)$  of the interior segment at force  $f = 0.3$ , with handles of length  $h = \ell_p$  (orange squares) and  $h = 2\ell_p$  (orange triangles). Blue dashed line: theoretical prediction for  $h = 0$  from Eq. (8). Orange solid line: theoretical prediction from Eq. (21) using  $\Delta(r; f) \approx \langle \mathbf{R}_{\text{handles}} \cdot \hat{\mathbf{r}} \rangle_{f=0; \mathbf{r}}$  extracted from MD simulation as input. Inset:  $\langle \mathbf{R}_{\text{handles}} \cdot \hat{\mathbf{r}} \rangle_{f=0; \mathbf{r}}$  as a function of  $r/L$  at  $h = \ell_p$ .

where for convenience we introduced the force-dependent partition function

$$Z(f) = \int_0^L dr' P_0(r') \frac{\sinh(\beta f(r' + \Delta(r'; f)))}{\beta f(r' + \Delta(r'; f))}. \quad (20)$$

Eq. (19) is structurally identical to Eq. (7) with the effective replacement  $r \mapsto r + \Delta(r; f)$ . The handles thus act as an  $r$ -dependent extension of the apparent end-to-end distance in the angular average, leaving the Boltzmann weight  $P_0(r)$  of the interior segment unaffected. The free energy follows as  $\beta F(r; f) = -\ln P(r; f)$ , in direct analogy with Eq. (8).

Although derived for short handles, this approximation also provides direct insight into the long-handle regime. When  $h \gg \ell_p$ , tangent-tangent correlations decay exponentially,  $\langle \mathbf{t}(s) \cdot \mathbf{t}(s') \rangle \sim e^{-|s-s'|/\ell_p}$ , so the handle orientation becomes decorrelated from  $\mathbf{r}$  beyond an arc-length of order  $\ell_p$  from the attachment point. The correction factor  $C[\mathbf{r}; \mathbf{f}]$  therefore loses its  $\mathbf{r}$ -dependence beyond this scale, and the residual coupling, confined to the first  $\sim \ell_p$  of each handle, saturates: increasing  $h$  beyond  $\ell_p$  adds no further  $\mathbf{r}$ -dependent contribution. This is precisely consistent with the simulation results of Fig. 4, where the free energies for  $h = \ell_p$  and  $h = 2\ell_p$  are almost indistinguishable. In this saturated regime, the distribution reduces to

$$P(r; f | h \gtrsim \ell_p) \approx \frac{P_0(r) \frac{\sinh(\beta f(r + \Delta(r; f | h = \ell_p)))}{\beta f(r + \Delta(r; f | h = \ell_p))}}{Z(f)}. \quad (21)$$

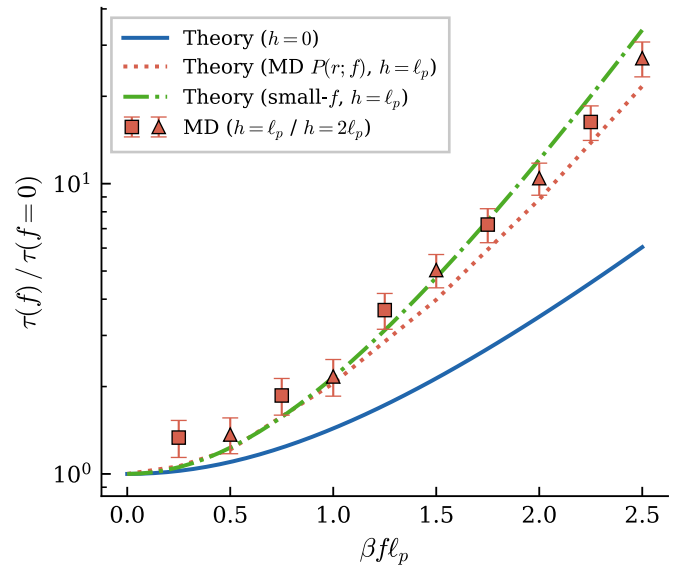


Figure 7. Force dependence of the looping time  $\tau(f)/\tau(f=0)$  as a function of  $\beta f \ell_p$ . Orange symbols: MD simulations with handles of length  $h = \ell_p$  (squares) and  $h = 2\ell_p$  (triangles). Blue solid line: no-handle theory ( $h = 0$ ). Orange dotted line: theory using  $F(r; f)$  extracted from MD with handles. Green dash-dotted line: small-force approximation using  $\langle \mathbf{R}_{\text{handles}} \cdot \hat{\mathbf{r}} \rangle_{f=0; \mathbf{r}}$  from a zero-force simulation.

Since typical experimental handles satisfy  $h \gg \ell_p$  [5], Eq. (21) is the experimentally relevant limit. The handles enter only through  $\Delta(r; f | h = \ell_p)$ , which shifts the argument of the sinh factor in  $r$ , modifying the force dependence of the looping time in a way that is independent of handle length, and in agreement with the simulations.

In Fig. 5, we validate this prediction against MD simulations. Using  $\Delta(r; f | h = \ell_p)$  extracted directly from simulation (shown in the inset) as input to Eq. (21), the resulting theoretical curve (orange solid line) is in excellent agreement with the simulation data for both  $h = \ell_p$  (orange squares) and  $h = 2\ell_p$  (orange triangles). This confirms that the handle correction is fully captured by the shift  $\Delta(r; f | h = \ell_p)$ , and that the modified free energy can be predicted accurately once  $\Delta$  is known. A note on the non-monotonic shape of  $\Delta(r; f | h = \ell_p)$  is given in Appendix C.

## V. SMALL-FORCE ANALYTICAL EXPANSION

The approach of the preceding section requires knowledge of  $\Delta$  at the force of interest, which was previously extracted directly from simulation. Here we show that in the limit of a small force, which is relevant to typical DNA looping experiments [5],  $\Delta$  can be expressed entirely in terms of a zero-force equilibrium average, requiring no finite-force simulation whatsoever.

Recall that the probability distribution of the interior segment in the presence of handles can be written as (Eqs. (15)

and (16))

$$\begin{aligned} \frac{P(\mathbf{r}; \mathbf{f})}{P_0(\mathbf{r})} &= e^{\beta \mathbf{f} \cdot \mathbf{r}} \left\langle e^{\beta \mathbf{f} \cdot \mathbf{R}_{\text{handles}}} \right\rangle_{f=0; \mathbf{r}} \\ &= e^{\beta f r \cos \theta_r} \left\langle e^{\beta f \mathbf{R}_{\text{handles}} \cdot \hat{\mathbf{z}}} \right\rangle_{f=0; \mathbf{r}}, \end{aligned} \quad (22)$$

where  $\theta_r$  is the angle between  $\mathbf{r}$  and the force axis. Since Eq. (21) was shown to be accurate (Fig. 5), the right-hand side can be approximated as

$$e^{\beta f r \cos \theta_r} \left\langle e^{\beta f \mathbf{R}_{\text{handles}} \cdot \hat{\mathbf{z}}} \right\rangle_{f=0; \mathbf{r}} \approx e^{\beta f (r + \Delta(r; f)) \cos \theta_r}, \quad (23)$$

from which we identify

$$\left\langle e^{\beta f \mathbf{R}_{\text{handles}} \cdot \hat{\mathbf{z}}} \right\rangle_{f=0; \mathbf{r}} \approx e^{\beta f \Delta(r; f) \cos \theta_r}. \quad (24)$$

We now expand both sides of Eq. (24) to first order in  $\beta f \Delta$ , which is valid when the force is sufficiently small that  $\beta f \Delta \ll 1$ . The right-hand side gives

$$e^{\beta f \Delta(r; f) \cos \theta_r} \approx 1 + \beta f \Delta(r; f) \cos \theta_r, \quad (25)$$

while expanding the left-hand side yields

$$\left\langle e^{\beta f \mathbf{R}_{\text{handles}} \cdot \hat{\mathbf{z}}} \right\rangle_{f=0; \mathbf{r}} \approx 1 + \beta f \langle \mathbf{R}_{\text{handles}} \cdot \hat{\mathbf{z}} \rangle_{f=0; \mathbf{r}}. \quad (26)$$

At zero force, isotropy implies that  $\langle \mathbf{R}_{\text{handles}} \rangle_{f=0; \mathbf{r}}$  is parallel to  $\mathbf{r}$ , so that

$$\langle \mathbf{R}_{\text{handles}} \cdot \hat{\mathbf{z}} \rangle_{f=0; \mathbf{r}} = \langle \mathbf{R}_{\text{handles}} \cdot \hat{\mathbf{r}} \rangle_{f=0; \mathbf{r}} \cos \theta_r. \quad (27)$$

Matching the two expansions, the  $\cos \theta_r$  factors cancel and we obtain

$$\Delta(r; f) \approx \langle \mathbf{R}_{\text{handles}} \cdot \hat{\mathbf{r}} \rangle_{f=0; \mathbf{r}}, \quad (28)$$

which is independent of  $f$ . Equation (28) is the central result of this section. The right-hand side requires only a zero-force simulation of the full construct: by tracking both  $\mathbf{r}$  and  $\mathbf{R}_{\text{handles}}$  along the trajectory and binning the projection  $\mathbf{R}_{\text{handles}} \cdot \hat{\mathbf{r}}$  as a function of  $r$ , one obtains  $\Delta$  directly. This can then be inserted into Eq. (21) to predict the force-dependent free energy and looping time without any simulation at finite force.

In the inset of Fig. 6, we present  $\langle \mathbf{R}_{\text{handles}} \cdot \hat{\mathbf{r}} \rangle_{f=0; \mathbf{r}}$  obtained from MD simulations at zero force and with  $h = \ell_p$ . This quantity was subsequently used as  $\Delta(r; f)$  in Eq. (21) to compute the free energy profile, shown as the solid orange line in the main panel, alongside the MD data for  $h = \ell_p$  and  $h = 2\ell_p$ . The theory is in excellent agreement with the simulation data. The free energy obtained within this small-force approximation was then used in Eq. (10) to evaluate the looping time, yielding the green curve in Fig. 7. For dimensionless forces  $\beta f \ell_p \lesssim 1$ , the predicted looping times are nearly indistinguishable from those obtained using the MD-derived free energy profiles, validating the small-force approximation in this regime.

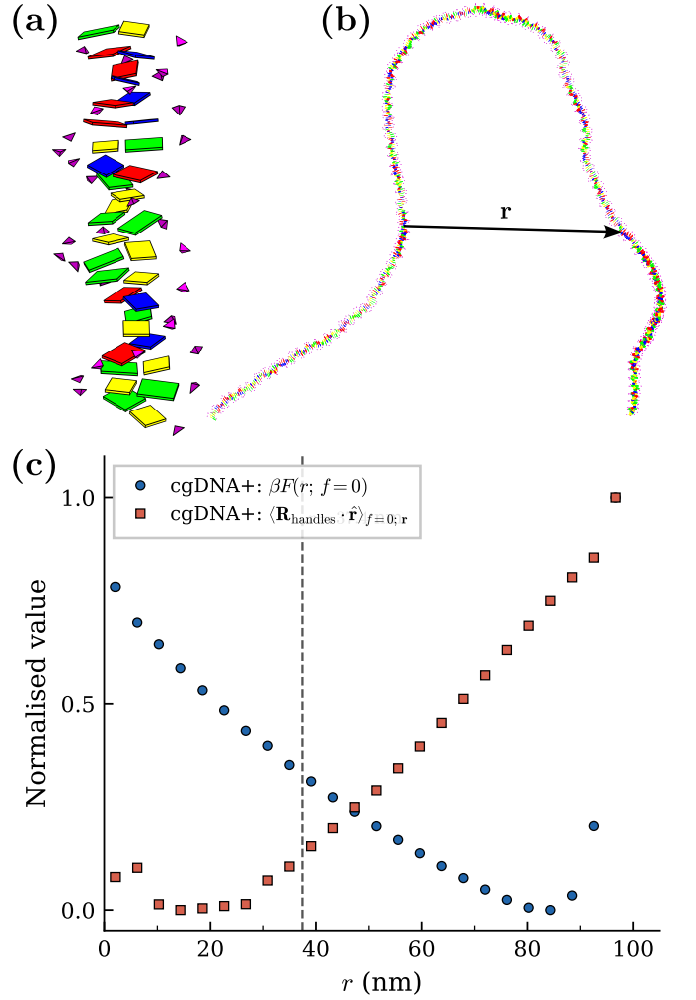


Figure 8. Illustration of the cgDNA+ model and extraction of the zero-force statistics. (a) The example sequence GCGACTCCGCGTCAATTC as rendered by cgDNA+. Bases are coloured by type: adenine (A, red), thymine (T, blue), cytosine (C, yellow), and guanine (G, green). Phosphate groups are shown as purple pyramids. (b) Representative Monte Carlo sample from cgDNA+ for a construct consisting of a 305 bp interior segment flanked by 150 bp handles on each side. The interior end-to-end vector  $\mathbf{r}$  is shown. (c) Zero-force free energy  $\beta F(r; f=0)$  (blue circles) and handle shift  $\Delta(r) = \langle \mathbf{R}_{\text{handles}} \cdot \hat{\mathbf{r}} \rangle_{f=0; \mathbf{r}}$  (orange squares), both normalised and plotted as a function of the interior end-to-end distance  $r$ , extracted from cgDNA+ Monte Carlo simulations. The dashed vertical line marks the value  $r = 37.4$  nm corresponding to the snapshot shown in panel (b).

## VI. COMPARISON TO EXPERIMENT VIA THE CGDNA+ MODEL

The previous sections established that DNA handles significantly affect the force dependence of the looping time, and developed a theoretical framework to account for this effect. We now validate the small-force expansion against the experimental data of Ref. [5], using the cgDNA+ model [26–28] to obtain the required zero-force statistics. cgDNA+ is a rigid-base coarse-grained model of DNA that treats phos-

phate groups explicitly (see Fig. 8(a)) and has been shown to reproduce the elastic properties of all-atom simulations with high fidelity [29]. Crucially, it allows efficient Monte Carlo sampling of equilibrium configurations for a given DNA sequence, from which the zero-force average  $\langle \mathbf{R}_{\text{handles}} \cdot \hat{\mathbf{r}} \rangle_{f=0; \mathbf{r}}$  of Eq. (28) can be extracted, without any finite-force simulation.

We consider a construct consisting of an interior segment of 305 base pairs, matching the loopable region in the experiment of Ref. [5], flanked by handles of 150 base pairs on each side, approximately equal to one persistence length. One such configuration is shown in Fig. 8(b). As the handles in the experiment are significantly longer, we can use this in the long-handle limit, Eq. (21). The zero-force free energy and the handle shift  $\langle \mathbf{R}_{\text{handles}} \cdot \hat{\mathbf{r}} \rangle_{f=0; \mathbf{r}}$  extracted from cgDNA+ Monte Carlo simulations are shown in Fig. 8(c), for a random sequence.

The resulting looping time predictions are shown in Fig. 9. The blue curve uses the cgDNA+ zero-force free energy in the no-handle theory, Eq. (7), and substantially underestimates the experimental data across the full force range. The green curve applies the small-force approximation, inserting the cgDNA+  $\Delta$  into Eq. (21). This prediction is in quantitative agreement with the experimental data of Ref. [5] throughout the small-force regime, and remains in reasonable agreement even upto 120 fN. These results demonstrate that the handle effect is not merely a theoretical curiosity: it is a dominant factor governing the force dependence of the looping time in this experiment, and our framework captures it quantitatively from first principles.

## VII. DISCUSSION AND CONCLUSION

We have systematically investigated how mechanical tension transmitted through flanking DNA segments affects the kinetics of DNA loop formation, a question relevant both to single-molecule force spectroscopy and to the broader problem of tension-dependent looping in gene regulation. Using molecular dynamics simulations of a wormlike chain, we demonstrated that handles of length  $h \sim \ell_p$  cause the normalised looping time  $\tau(f)/\tau(0)$  to increase substantially more steeply with force than predicted by the standard theory. The effect saturates once  $h \gtrsim \ell_p$  — the free energies for  $h = \ell_p$  and  $h = 2\ell_p$  are almost indistinguishable — and vanishes entirely when the junction between handle and looping segment is made flexible, confirming that the effect is of orientational origin.

We showed that all of these observations are encoded in the effective free energy landscape of the interior segment, and developed an analytical framework to capture them. Starting from the path-integral expression for the radial distribution of the interior segment, we identified a handle correction factor  $C[\mathbf{r}; \mathbf{f}]$  that modulates the no-handle result. In the experimentally relevant limit  $h \gtrsim \ell_p$ , this reduces to a shift  $\Delta(r; f)$  in the argument of the sinh factor entering the orientational average, yielding a modified free energy that can be inserted directly into the Szabo–Schulten–Schulten looping time formula with-

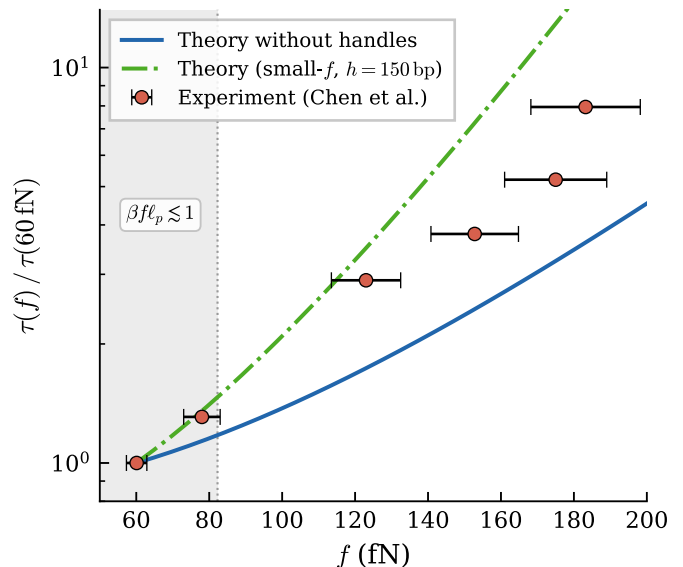


Figure 9. Force dependence of the looping time, normalised by its value at  $f = 60$  fN, as a function of the applied force. Blue solid line: theoretical prediction without handles, Eq. (7), using the cgDNA+ zero-force free energy as input. Green dashed line: small-force approximation including handles, Eq. (21), using  $\langle \mathbf{R}_{\text{handles}} \cdot \hat{\mathbf{r}} \rangle_{f=0; \mathbf{r}}$  extracted from cgDNA+ at zero force. Orange circles: experimental data from Ref. [5]. The shaded region indicates the small-force regime  $\beta f \ell_p \lesssim 1$ . The no-handle theory substantially underestimates the data, while the handle theory agrees quantitatively with experiment up to around 120 fN.

out additional free parameters. When  $\Delta$  is taken from MD simulation, the resulting free energy and looping time are in very good agreement with the simulation data.

To determine  $\Delta$  without finite-force simulations, we derived a small-force expansion showing that  $\Delta$  reduces to a zero-force equilibrium average of the handle extension projected onto the interior segment direction. This quantity can be extracted from zero-force simulations alone, after which the entire force dependence of the looping time follows analytically. Applying this approach to the cgDNA+ model, we obtained predictions in quantitative agreement with experimental data, an agreement that prior theories neglecting the handle effect could not achieve [11].

Taken together, our results establish that the geometry of force transmission has a significant and predictable effect on looping kinetics. In optical-tweezer experiments this effect must be accounted for to correctly interpret measured looping times. More broadly, in biological settings where DNA is under tension from transcription, supercoiling, or chromatin organisation, the force is similarly transmitted to looping sites through flanking segments rather than acting on them directly. The same reasoning applies directly to the folding and unfolding of nucleic-acid hairpins in optical-tweezer assays [6, 7]. The mechanism may also bear on the emerging picture of chromosome architecture, in which chromatin loops have been proposed to form via passive diffusive capture of anchor sites, as an alternative to active, motor-driven extrusion [19, 20]. By making explicit how tension is physically

propagated through the flanking polymer, our framework offers a quantitative route to test whether such diffusive capture is sensitive to the mechanical loading of the surrounding chromatin. Our framework provides a quantitative route to assess and correct for this effect in both contexts, and suggests that the force dependence of looping kinetics in gene regulatory systems may be substantially stronger than predicted by models that assume direct force application.

## DATA AVAILABILITY

The simulation data and analysis code that support the findings of this article will be made openly available upon publication.

## ACKNOWLEDGMENTS

This research is financially supported by the Dutch Ministry of Education, Culture and Science (Gravitation Program 024.005.020 – Interactive Polymer Materials IPM).

- 
- [1] M. T. Halma and L. Xu, Life under tension: the relevance of force on biological polymers, *Biophysics Reports* **10**, 48 (2024).
- [2] F. M. Fazal and S. M. Block, Optical tweezers study life under tension, *Nature photonics* **5**, 318 (2011).
- [3] S. B. Smith, L. Finzi, and C. Bustamante, Direct mechanical measurements of the elasticity of single dna molecules by using magnetic beads, *Science* **258**, 1122 (1992).
- [4] F. Kriegel, W. Vanderlinden, T. Nicolaus, A. Kardinal, and J. Lipfert, Measuring single-molecule twist and torque in multiplexed magnetic tweezers, in *Nanoscale Imaging: Methods and Protocols* (Springer, 2018) pp. 75–98.
- [5] Y.-F. Chen, J. Milstein, and J.-C. Meiners, Protein-mediated dna loop formation and breakdown in a fluctuating environment, *Physical Review Letters* **104**, 258103 (2010).
- [6] J.-D. Wen, M. Manosas, P. T. Li, S. B. Smith, C. Bustamante, F. Ritort, and I. Tinoco, Force unfolding kinetics of rna using optical tweezers. i. effects of experimental variables on measured results, *Biophysical journal* **92**, 2996 (2007).
- [7] M. Manosas, J.-D. Wen, P. T. Li, S. B. Smith, C. Bustamante, I. Tinoco, and F. Ritort, Force unfolding kinetics of rna using optical tweezers. ii. modeling experiments, *Biophysical journal* **92**, 3010 (2007).
- [8] M. T. Woodside and S. M. Block, Reconstructing folding energy landscapes by single-molecule force spectroscopy, *Annual review of biophysics* **43**, 19 (2014).
- [9] A. Szabo, K. Schulten, and Z. Schulten, First passage time approach to diffusion controlled reactions, *The Journal of chemical physics* **72**, 4350 (1980).
- [10] J. Shin and W. Sung, Effects of static and temporally fluctuating tensions on semiflexible polymer looping, *The Journal of Chemical Physics* **136** (2012).
- [11] W. Laeremans and W. G. Ellenbroek, Theoretical models for tension-dependent dna looping time, *Physical Review Research* **7**, L032041 (2025).
- [12] J. Milstein and J.-C. Meiners, On the role of dna biomechanics in the regulation of gene expression, *Journal of The Royal Society Interface* **8**, 1673 (2011).
- [13] S. Blumberg, A. V. Tkachenko, and J.-C. Meiners, Disruption of protein-mediated dna looping by tension in the substrate dna, *Biophysical journal* **88**, 1692 (2005).
- [14] Y.-F. Chen, J. Milstein, and J.-C. Meiners, Femtonewton entropic forces can control the formation of protein-mediated dna loops, *Physical review letters* **104**, 048301 (2010).
- [15] R. Schleif, Dna looping, *Annual review of biochemistry* **61**, 199 (1992).
- [16] J. F. Allemand, S. Cocco, N. Douarche, and G. Lia, Loops in dna: an overview of experimental and theoretical approaches, *The European Physical Journal E* **19**, 293 (2006).
- [17] K. Matthews, Dna looping, *Microbiological reviews* **56**, 123 (1992).
- [18] F. Gallet, D. Arcizet, P. Bohec, and A. Richert, Power spectrum of out-of-equilibrium forces in living cells: amplitude and frequency dependence, *Soft matter* **5**, 2947 (2009).
- [19] T. Gerguri, X. Fu, Y. Kakui, B. S. Khatri, C. Barrington, P. A. Bates, and F. Uhlmann, Comparison of loop extrusion and diffusion capture as mitotic chromosome formation pathways in fission yeast, *Nucleic acids research* **49**, 1294 (2021).
- [20] F. Uhlmann, A unified model for cohesin function in sister chromatid cohesion and chromatin loop formation, *Molecular Cell* **85**, 1058 (2025).
- [21] W. Laeremans, A. F. den Ouden, J. Hooyberghs, and W. G. Ellenbroek, Polymer dynamics under tension: Mean first passage time for looping, *Physical Review E* **111**, 025401 (2025).
- [22] O. Kratky and G. Porod, Röntgenuntersuchung gelöster fadenmoleküle, *Recueil des Travaux Chimiques des Pays-Bas* **68**, 1106 (1949).
- [23] J. F. Marko and E. D. Siggia, Stretching dna, *Macromolecules* **28**, 8759 (1995).
- [24] J. Wilhelm and E. Frey, Radial distribution function of semiflexible polymers, *Physical review letters* **77**, 2581 (1996).
- [25] J. Bhattacharjee, D. Thirumalai, and J. Bryngelson, Distribution function of the end-to-end distance of semiflexible polymers, *arXiv preprint cond-mat/9709345* (1997).
- [26] A. S. Patelli, *A sequence-dependent coarse-grain model of B-DNA with explicit description of bases and phosphate groups parametrised from large scale Molecular Dynamics simulations*, Ph.D. thesis, EPFL, Lausanne (2019).
- [27] D. Petkevičiūtė, M. Pasi, O. Gonzalez, and J. Maddocks, cgDNA: a software package for the prediction of sequence-dependent coarse-grain free energies of B-form DNA, *Nucl. Acids Res.* **42**, e153 (2014).
- [28] R. Sharma, A. S. Patelli, L. De Bruin, and J. H. Maddocks, cgNA+ web: A visual interface to the cgNA+ sequence-dependent statistical mechanics model of double-stranded nucleic acids, *J. Mol. Biol.* , 167978 (2023).
- [29] W. Laeremans, M. Segers, A. Voorspoels, E. Carlon, and J. Hooyberghs, Insights into elastic properties of coarse-grained dna models: q-stiffness of cgdna vs cgdna+, *The Journal of Chemical Physics* **160** (2024).
- [30] A. P. Thompson, H. M. Aktulga, R. Berger, D. S. Bolintineanu, W. M. Brown, P. S. Crozier, P. J. in 't Veld, A. Kohlmeyer, S. G.

Moore, T. D. Nguyen, R. Shan, M. J. Stevens, J. Tranchida, C. Trott, and S. J. Plimpton, LAMMPS - a flexible simulation tool for particle-based materials modeling at the atomic, meso, and continuum scales, *Comp. Phys. Comm.* **271**, 108171 (2022).

- [31] M. Hijazi, D. M. Wilkins, and M. Ceriotti, Fast-forward langevin dynamics with momentum flips, *The Journal of chemical physics* **148** (2018).
- [32] W. Laeremans, Wlaeremans/polymer-looping-under-tension-fjc-: Code and data polymer looping under tension fjc (2025).
- [33] W. Laeremans, Wlaeremans/polymer-looping-under-tension-wlc: Code and data polymer looping under tension wlc (2025).

## Appendix A: Simulation details

Molecular dynamics simulations were performed using the LAMMPS software [30] in dimensionless Lennard-Jones units with inverse temperature  $\beta = (k_B T)^{-1} = 1$ .

### Polymer model

The polymer was modelled as a bead-spring chain of  $N + 1$  beads with equilibrium bond length  $b = 0.5$  and bead mass  $m = 1$ . Consecutive beads were connected by harmonic bonds,

$$U_{\text{bond}} = \frac{K}{2} \sum_{i=0}^{N-1} (|\mathbf{r}_{i+1} - \mathbf{r}_i| - b)^2, \quad (\text{A1})$$

with stiffness  $K = 10^4$ , ensuring that bond length fluctuations remain small compared to  $b$ . Bending rigidity was introduced via

$$U_{\text{bend}} = \frac{\kappa}{2} \sum_{i=1}^{N-1} \theta_i^2, \quad (\text{A2})$$

where  $\theta_i$  is the angle between consecutive bond vectors and  $\kappa = 10$ . The persistence length is then  $\ell_p = \beta \kappa b = 5$  in dimensionless units, corresponding to approximately 50nm in physical units [10, 11]. An equal and opposite force along the  $z$ -axis was applied to the two terminal beads to impose tension.

### Equilibration and integration

Starting from a straight configuration, each system was equilibrated for  $10^8$  timesteps using Langevin dynamics (`fix langevin` in LAMMPS) with initial velocities drawn from a Gaussian distribution at unit temperature and a timestep of 0.005. Production runs were subsequently performed using the fast-forward Langevin integrator (`fix ffl`) [31] with the same timestep and friction coefficient  $\gamma = 1$ .

## Looping times and free energy sampling

The looping time and effective free energy were determined following the procedures described in Refs. [32, 33], to which we refer the reader for full details. Every simulation data point in this work is the average over 100 independent simulations.

### cgDNA+ Monte Carlo simulations

We sampled the zero-force free energy for a system consisting of a 305 bp interior segment flanked by 150 bp handles on each side, using the cgDNA+ parameter set (cgDNA+ps1.mat) [26–28]. To generate independent samples of the DNA configuration, we employed direct Monte Carlo sampling by drawing configurations from a multivariate Gaussian distribution. We collected  $10^5$  samples for a random sequence. The choice of random sequence is inconsequential for this study: we verified that results are insensitive to the specific sequence composition by testing multiple random sequences of the same length. The cgDNA+ software is available at: [https://github.com/rahu12512/cgDNA\\_plus\\_Matlab](https://github.com/rahu12512/cgDNA_plus_Matlab).

## Appendix B: Derivation of the handle correction factor

We derive Eqs. (15) and (16) starting from Eq. (14). Using the decomposition  $\mathbf{R}_{\text{tot}} = \mathbf{r} + \mathbf{R}_{\text{handles}}$ , the numerator of Eq. (14) factorises as

$$\begin{aligned} & \int \mathcal{D}[\mathbf{t}] \delta(\mathbf{r} - \mathbf{r}[\mathbf{t}]) e^{-\beta \mathcal{H}_0[\mathbf{t}] + \beta \mathbf{f} \cdot \mathbf{R}_{\text{tot}}[\mathbf{t}]} \\ &= e^{\beta \mathbf{f} \cdot \mathbf{r}} \int \mathcal{D}[\mathbf{t}] \delta(\mathbf{r} - \mathbf{r}[\mathbf{t}]) e^{-\beta \mathcal{H}_0[\mathbf{t}] + \beta \mathbf{f} \cdot \mathbf{R}_{\text{handles}}[\mathbf{t}]}, \end{aligned} \quad (\text{B1})$$

where the factor  $e^{\beta \mathbf{f} \cdot \mathbf{r}}$  has been pulled outside the integral using the delta function constraint  $\mathbf{r}[\mathbf{t}] = \mathbf{r}$ . Multiplying and dividing by  $P_0(\mathbf{r})$ , defined as

$$P_0(\mathbf{r}) = \frac{\int \mathcal{D}[\mathbf{t}] \delta(\mathbf{r} - \mathbf{r}[\mathbf{t}]) e^{-\beta \mathcal{H}_0[\mathbf{t}]}}{\int \mathcal{D}[\mathbf{t}] e^{-\beta \mathcal{H}_0[\mathbf{t}]}} \quad (\text{B2})$$

the numerator becomes proportional to

$$e^{\beta \mathbf{f} \cdot \mathbf{r}} P_0(\mathbf{r}) C[\mathbf{r}; \mathbf{f}], \quad (\text{B3})$$

where we define the handle correction factor

$$\begin{aligned} C[\mathbf{r}; \mathbf{f}] &\equiv \frac{\int \mathcal{D}[\mathbf{t}] \delta(\mathbf{r} - \mathbf{r}[\mathbf{t}]) e^{-\beta \mathcal{H}_0[\mathbf{t}] + \beta \mathbf{f} \cdot \mathbf{R}_{\text{handles}}[\mathbf{t}]}}{\int \mathcal{D}[\mathbf{t}] \delta(\mathbf{r} - \mathbf{r}[\mathbf{t}]) e^{-\beta \mathcal{H}_0[\mathbf{t}]}} \\ &= \left\langle e^{\beta \mathbf{f} \cdot \mathbf{R}_{\text{handles}}} \right\rangle_{f=0; \mathbf{r}}. \end{aligned} \quad (\text{B4})$$

This is the zero-force conditional average of the handle Boltzmann weight, with the interior segment's end-to-end vector fixed at  $\mathbf{r}$ . Substituting into Eq. (14) and performing the same decomposition in the denominator yields Eq. (15).

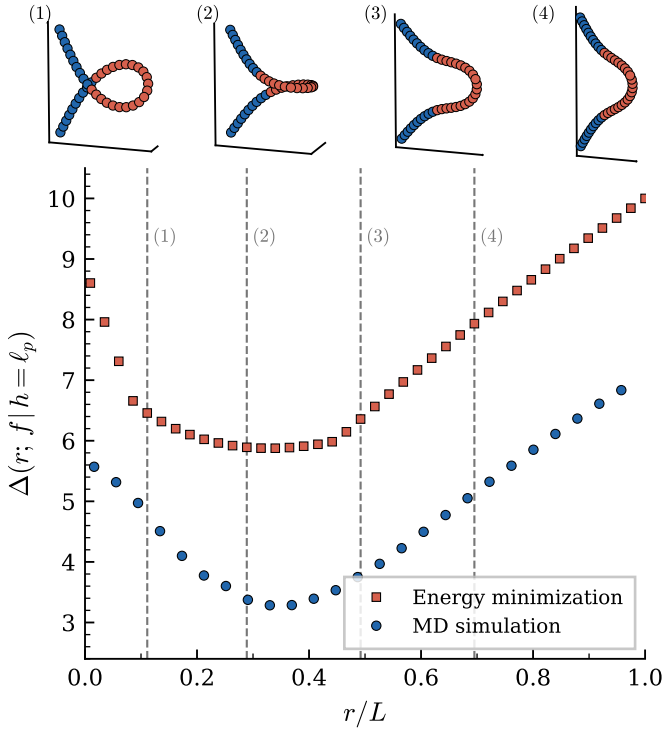


Figure 10. Bottom panel:  $\Delta(r; f | h = \ell_p)$  as a function of  $r/L$  for handles of length  $h = \ell_p$  at force  $f = 0.3$ . Blue circles: MD simulation. Orange squares: energy-minimized estimate. Vertical dashed lines mark the four values of  $r/L$  at which representative minimized configurations are shown in the top panel. Top panel: minimum-energy chain conformations at the indicated values of  $r/L$ . Blue beads: handle segments; orange beads: interior segment. The configurations illustrate the conformational progression from a planar loop at small  $r/L$ , through an out-of-plane twisted geometry, back to a planar and nearly straight conformation at large  $r/L$ .

### Appendix C: Non-monotonic shape of $\Delta$ and alignment

The shift function  $\Delta(r; f)$  extracted from MD simulation exhibits a pronounced non-monotonic dependence on the interior end-to-end distance  $r$ , as was shown in Fig. 5 of the main text. It is large at small  $r$ , decreases to a minimum at intermediate  $r$ , and rises again as  $r$  approaches the contour length. The origin of this behaviour is not immediately obvious from the definition of  $\Delta$ , and we show here that it can be traced back to a transition in the polymer configurations.

To this end, we perform a constrained minimization of the force-dependent Hamiltonian  $\mathcal{H}_f$ , imposing that the interior end-to-end distance is fixed at a prescribed value  $r$ . For each  $r$ , the minimum-energy chain conformation is computed under the constraint  $|\mathbf{r}| = r$ , and we extract

$$\Delta(r; f | h = \ell_p) = R_{\text{tot}} - r. \quad (\text{C1})$$

This energy-minimized  $\Delta$  neglects thermal fluctuations and therefore differs from the MD estimate in absolute magnitude. Nevertheless, as shown in the bottom panel of Fig. 10, the  $r$ -dependence of the two estimates is strikingly similar, demonstrating that the shape of  $\Delta(r; f)$  is governed by the energy-

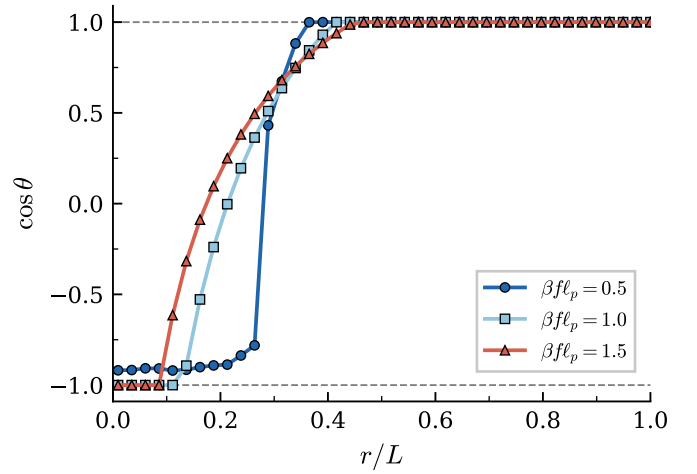


Figure 11. Alignment between inner looping segment  $\mathbf{r}$  and total end-to-end direction  $\mathbf{R}_{\text{tot}}$  versus normalized end-to-end distance  $r/L$ , measured as  $\cos \theta$ , with  $\theta$  the angle between the two vectors. At low and high  $r$ , the vectors are (anti)parallel; at intermediate  $r$ , the loop twists out of plane (see Fig. 10). Alignment improves at lower forces, as discussed in the main text.

minimizing configurations and is not a thermal fluctuation effect.

The top panel of Fig. 10 shows representative minimized configurations at four values of  $r/L$ , marked by the vertical dashed lines in the bottom panel. These configurations reveal the conformational progression underlying the shape of  $\Delta$ . At small  $r/L$ , the polymer forms a nearly planar loop in which both handles point predominantly along the force axis, resulting in a large  $\Delta$ . The inner segment and total end-to-end direction are (anti)parallel at these configurations. As  $r/L$  increases, the chain is forced to twist out of plane to accommodate the growing interior distance while maintaining the handle alignment, and  $\Delta$  decreases. This out-of-plane twist causes the inner and total directions to become misaligned. At large  $r/L$ , the conformation returns to a planar geometry and the chain approaches full extension, causing  $\Delta$  to rise again as the handles straighten along the force direction. The inner segment realigns with  $\mathbf{R}_{\text{tot}}$ .

To quantify this alignment throughout the conformational sequence, we compute the cosine of the angle between  $\mathbf{r}$  and  $\mathbf{R}_{\text{tot}}$  as a function of  $r/L$  (Fig. 11). As expected,  $\cos \theta$  is large (near  $\pm 1$ ) at small and large  $r/L$  where the conformation is planar, and drops to intermediate values at intermediate  $r/L$  where the loop twists out of plane. The non-monotonic shape of  $\Delta(r; f)$  is therefore a direct consequence of this conformational sequence, which is linked to the directional alignment between the looping region and the global extension. Notably, Fig. 11 shows that this alignment is more pronounced at lower forces, suggesting that our theoretical framework, which relies on this alignment assumption via Eq. 17, is particularly valid in the experimentally relevant low-force regime.

### Appendix D: Low-force expansion of the partition function

In Appendix C, it was shown that for low forces and most values of  $r$ , the vectors  $\mathbf{r}$  and  $\mathbf{R}_{\text{tot}}$  are aligned. Here, we demonstrate this more explicitly by expanding the partition function to first order in the force  $f$ .

#### Factoring out the end-to-end vector contribution

The constrained partition function can be written as

$$Z(\mathbf{r}, f) = \int \mathcal{D}[\mathbf{t}] \delta(\mathbf{r} - \mathbf{r}[\mathbf{t}]) \exp(-\beta \mathcal{H}_0[\mathbf{t}] + \beta \mathbf{f} \cdot \mathbf{R}_{\text{tot}}[\mathbf{t}]). \quad (\text{D1})$$

Since  $\mathbf{R}_{\text{tot}} = \mathbf{r} + \mathbf{R}_{\text{handles}}$  and the delta function fixes  $\mathbf{r}[\mathbf{t}] = \mathbf{r}$ , we can factor out the contribution of the end-to-end vector:

$$Z(\mathbf{r}, f) = e^{\beta \mathbf{f} \cdot \mathbf{r}} \times \int \mathcal{D}[\mathbf{t}] \delta(\mathbf{r} - \mathbf{r}[\mathbf{t}]) \exp(-\beta \mathcal{H}_0[\mathbf{t}] + \beta \mathbf{f} \cdot \mathbf{R}_{\text{handles}}[\mathbf{t}]). \quad (\text{D2})$$

Choosing the force along  $\hat{\mathbf{z}}$  and writing  $\mathbf{f} = f\hat{\mathbf{z}}$ , so that  $\mathbf{f} \cdot \mathbf{r} = fr \cos \theta$ , this becomes

$$Z(\mathbf{r}, f) = e^{\beta fr \cos \theta} \times \int \mathcal{D}[\mathbf{t}] \delta(\mathbf{r} - \mathbf{r}[\mathbf{t}]) \exp(-\beta \mathcal{H}_0[\mathbf{t}] + \beta f \hat{\mathbf{z}} \cdot \mathbf{R}_{\text{handles}}[\mathbf{t}]). \quad (\text{D3})$$

#### Rewriting as a thermal average

Multiplying and dividing by the zero-force partition function  $Z(\mathbf{r}, 0)$ , we recognise the remaining path integral as a thermal average at  $f = 0$ :

$$Z(\mathbf{r}, f) = e^{\beta fr \cos \theta} Z(\mathbf{r}, 0) \langle \exp(\beta f \hat{\mathbf{z}} \cdot \mathbf{R}_{\text{handles}}[\mathbf{t}]) \rangle_{\mathbf{r}, f=0}. \quad (\text{D4})$$

#### First-order expansion in $f$

Expanding the exponential inside the average to first order in  $f$ :

$$\left\langle e^{\beta f \hat{\mathbf{z}} \cdot \mathbf{R}_{\text{handles}}} \right\rangle_{\mathbf{r}, f=0} = 1 + \beta f \hat{\mathbf{z}} \cdot \langle \mathbf{R}_{\text{handles}} \rangle_{\mathbf{r}, f=0} + \mathcal{O}(f^2). \quad (\text{D5})$$

By spherical symmetry at  $f = 0$ , the average of any vector quantity must point along  $\hat{\mathbf{r}}$ . We therefore write

$$\langle \mathbf{R}_{\text{handles}} \rangle_{\mathbf{r}, f=0} = \Delta(r) \hat{\mathbf{r}}, \quad \Delta(r) \equiv \langle \mathbf{R}_{\text{handles}} \cdot \hat{\mathbf{r}} \rangle_{\mathbf{r}, f=0}, \quad (\text{D6})$$

so that  $\hat{\mathbf{z}} \cdot \langle \mathbf{R}_{\text{handles}} \rangle = \Delta(r) \cos \theta$ . Substituting into Eq. (D5) and re-exponentiating to first order in  $f$ :

$$\begin{aligned} \left\langle e^{\beta f \hat{\mathbf{z}} \cdot \mathbf{R}_{\text{handles}}} \right\rangle_{\mathbf{r}, f=0} &= 1 + \beta f \Delta(r) \cos \theta + \mathcal{O}(f^2) \\ &= e^{\beta f \Delta(r) \cos \theta} + \mathcal{O}(f^2). \end{aligned} \quad (\text{D7})$$

**Resulting partition function**

Inserting Eq. (D7) into Eq. (D4), and using spherical symmetry to write  $Z(\mathbf{r}, 0) = Z(r, 0)/(4\pi r^2)$ :

$$Z(\mathbf{r}, f) = \frac{Z(r, 0)}{4\pi r^2} e^{\beta f (r + \Delta(r)) \cos \theta}. \quad (\text{D8})$$

The effective length  $r + \Delta(r)$  combines the end-to-end distance  $r$  with the mean handle extension  $\Delta(r)$  projected along  $\hat{\mathbf{r}}$ .

#### Marginal partition function and alignment

Integrating over all orientations gives the marginal (scalar) partition function:

$$\begin{aligned} Z(r, f) &= \int_0^{2\pi} d\phi \int_0^\pi d\theta r^2 \sin \theta Z(\mathbf{r}, f) \\ &= \frac{Z(r, 0)}{4\pi} \int_0^{2\pi} d\phi \int_0^\pi d\theta \sin \theta e^{\beta f (r + \Delta(r)) \cos \theta} \\ &= Z(r, 0) \int_0^\pi d\theta \frac{\sin \theta}{2} e^{\beta f (r + \Delta(r)) \cos \theta} \\ &= Z(r, 0) \frac{\sinh[\beta f (r + \Delta(r))]}{\beta f (r + \Delta(r))}, \end{aligned} \quad (\text{D9})$$

which is the standard Langevin form with an effective length  $r + \Delta(r)$ .

This confirms that  $\mathbf{r}$  and  $\mathbf{R}_{\text{tot}}$  are, on average, parallel. The parallelism originates from the  $f = 0$  symmetry argument: since there is no external direction singled out at zero force,  $\langle \mathbf{R}_{\text{handles}} \rangle_{\mathbf{r}, f=0}$  can only point along  $\hat{\mathbf{r}}$ , the direction of  $\mathbf{r}$  itself. Consequently,  $\langle \mathbf{R}_{\text{tot}} \rangle = \mathbf{r} + \langle \mathbf{R}_{\text{handles}} \rangle = (r + \Delta(r)) \hat{\mathbf{r}}$  is simply a rescaling of  $\mathbf{r}$ , not a vector at some independent angle. The low-force expansion in  $f$  shows this structure is preserved when the force is turned on: the orientational weight in Eq. (D8) depends on  $\theta$  only through the combined effective length  $r + \Delta(r)$ , consistent with  $\mathbf{r}$  and  $\mathbf{R}_{\text{tot}}$  remaining collinear to  $\mathcal{O}(f^2)$ .